Structure of Kα1,2- and Kβ1,3-emission x-ray spectra for Se, Y, and Zr

Y. Ito, T. Tochio, M. Yamashita, S. Fukushima, A. Vlaicu, J. Marques, J. Sampaio, M. Guerra, J. Santos, Ł. Syrocki, et al.

▶ **To cite this version:**

Y. Ito, T. Tochio, M. Yamashita, S. Fukushima, A. Vlaicu, et al.. Structure of Kα1,2- and Kβ1,3-emission x-ray spectra for Se, Y, and Zr. Physical Review A, 2020, 102 (5), pp.052820. 10.1103/PhysRevA.102.052820 . hal-04553916

HAL Id: hal-04553916
https://hal.science/hal-04553916

Submitted on 30 Apr 2024

HAL is a multi-disciplinary open access archive for the deposit and dissemination of scientific research documents, whether they are published or not. The documents may come from teaching and research institutions in France or abroad, or from public or private research centers.

L'archive ouverte pluridisciplinaire **HAL**, est destinée au dépôt et à la diffusion de documents scientifiques de niveau recherche, publiés ou non, émanant des établissements d'enseignement et de recherche français ou étrangers, des laboratoires publics ou privés.

Structure of $K\alpha_{1,2}$- and $K\beta_{1,3}$-emission x-ray spectra for Se, Y, and Zr

Y. Ito,[1,*] T. Tochio,[2] M. Yamashita,[3] S. Fukushima,[4] A. M. Vlaicu,[5] J. P. Marques,[6,7] J. M. Sampaio,[8] M. Guerra,[7] J. P. Santos,[7] Ł. Syrocki,[9] K. Słabkowska,[9] E. Węder,[9] M. Polasik,[9] J. Rzadkiewicz,[10] P. Indelicato,[11] Y. Ménesguen,[12] M.-Ch. Lépy,[12] and F. Parente[7,13,†]

[1]*Laboratory of Atomic and Molecular Physics, ICR, Kyoto University, Gokasho, Uji, Kyoto 611-0011 Japan*
[2]*Department of Physics, Faculty of Science, Kobe University, 1-1 Rokkodai, Kobe 657-8501, Japan*
[3]*HIT, 3-1-12 Yukihira, Suma-ku, Kobe 654-0037, Japan*
[4]*Kobe Material Testing Laboratory Company, Ltd., 47-13 Nijima, Harima-cho, Kako-gun, Hyogo 675-0155, Japan*
[5]*National Institute of Materials Physics, Bucharest-Magurele, Str. Atomistilor 405A, P.O. Box MG-7, 077125 Magurele-Ilfov, Romania*
[6]*BioISI-Biosystems & Integrative Sciences Institute, Faculty of Sciences, University of Lisboa, 1749-016 Lisboa, Portugal*
[7]*Departamento de Física, Laboratório de Instrumentação, Engenharia Biomédica e Física da Radiação (LIBPhys-UNL), Faculdade de Ciências e Tecnologia da Universidade Nova de Lisboa, Monte da Caparica, 2892-516 Caparica, Portugal*
[8]*LIP-Laboratório de Instrumentação e Física Experimental de Partículas, Avenida Professor Gama Pinto 2, 1649-003 Lisboa, Portugal*
[9]*Faculty of Chemistry, Nicolaus Copernicus University in Toruń, Gagarina 7, 87-100 Toruń, Poland*
[10]*National Centre for Nuclear Research, 05-400 Otwock, Poland*
[11]*Laboratoire Kastler Brossel, Sorbonne Université, CNRS, ENS-PSL Research University, Collège de France, Case 74; 4, place Jussieu, F-75005 Paris, France*
[12]*Université Paris-Saclay, CEA, LIST, Laboratoire National Henri Becquerel (LNE-LNHB), F-91120 Palaiseau, France*
[13]*BioISI–Biosystems & Integrative Sciences Institute, Faculdade de Ciências da Universidade de Lisboa, Campo Grande, C8, 1749-016 Lisboa, Portugal*

(Received 27 April 2020; revised 15 September 2020; accepted 20 October 2020; published 20 November 2020)

The $K\alpha$ and $K\beta$ x-ray spectra of Se, Y, and Zr were studied experimentally and theoretically in order to obtain information on the $K\alpha_1$ line asymmetry and the spin doublet in $K\beta_{1,3}$ diagram lines. Using a high-resolution antiparallel double-crystal x-ray spectrometer, we obtained the line shapes, that is, asymmetry index and natural linewidths. We found that the corrected full width at half maximum of the $K\alpha_1$ and $K\alpha_2$ lines as a function of Z is in good agreement with the data in the literature. Furthermore, satellite lines arising from shake-off appear in the low-energy side of the $K\alpha_1$ and $K\alpha_2$ lines in Se but, in Y and Zr, it was very difficult to identify the contribution of the shake process to the overall lines. The $K\beta_{1,3}$ natural linewidth of these elements was also corrected using the appropriate instrumental function for this type of x-ray spectrometer, and the spin doublet energies were obtained from the peak positions. The corrected full width at half maximum (FWHM) of the $K\beta_1$ x-ray lines increases linearly with Z, but this tendency was found to be, in general, not linear for $K\beta_3$ x-ray lines. This behavior may be due to the existence of satellite lines originated from shake processes. Simulated line profiles, obtained using the multiconfiguration Dirac-Fock formalism, accounting for radiative and radiationless transitions and shake-off processes, show a very good agreement with the high-resolution experimental spectra.

DOI: 10.1103/PhysRevA.102.052820

I. INTRODUCTION

The $K\alpha$ and $K\beta$ x-ray emission spectra of the $3d$ transition metals exhibit several peculiar asymmetric line profiles not observed in other elements [1], whose origin has been under investigation and debate [2–6]. Several mechanisms, such as shake processes [7], conduction-band collective excitation [8], exchange [9–15], and final-state interactions [16,17] were suggested to account for this effect. In particular, Deutsch and co-workers [4,5], Hölzer *et al.* [6], Anagnostopoulos *et al.* [18], Chantler *et al.* [19], and Ito *et al.* [20] suggested that the line shapes in $K\alpha_{1,2}$ x-ray spectra could be accounted for by the diagram transition and $3s$, $3p$, and $3d$ spectator-hole transitions. Ito *et al.* [20] measured systematically the $K\alpha_{1,2}$ spectra in the elements from Ca to Ge using an antiparallel two-crystal x-ray spectrometer and elucidated the origin of the asymmetry in the $K\alpha_1$ emission profile, confirming that the broadening of the linewidths of $K\alpha_2$ spectra originates from L_2-$L_3M_{4,5}$ Coster-Kronig transitions. Combined *ab initio* Dirac-Fock calculations and high-resolution x-ray emission measurements of $K\alpha_{1,2}$ spectra for elements Ca, Ti, and Ge show that the asymmetric line shapes of these emission lines

*Present address: Rigaku Corporation, 14-8, Akaoji-cho, Takatsuki-shi, Osaka 569-1146, Japan.
†Corresponding author: facp@fct.unl.pt

Published by the American Physical Society under the terms of the Creative Commons Attribution 4.0 International license. Further distribution of this work must maintain attribution to the author(s) and the published article's title, journal citation, and DOI.

TABLE I. Experimental conditions of the measurements using a two-crystal x-ray spectrometer. The measurements were performed with a tube voltage of 40 kV and the current of 60 mA under vacuum. The analyzing crystal was Si(220).

Element	Specimen	line	Accumulation time (s/point)	2θ step (°)
Se	Metal	$K\alpha_{1,2}$	7	0.0005
		$K\beta_{1,2,3}$	45	0.001
Y	Metal	$K\alpha_{1,2}$	18	0.0005
		$K\beta_{1,2,3}$	120	0.002
Zr	Metal	$K\alpha_{1,2}$	17	0.0005
		$K\beta_{1,3}$	120	0.0005

can be fully explained by considering only the diagram and the $3d$ spectator transitions [20].

On the other hand, the $K\beta_{1,3}$ x-ray emission spectrum includes $K\beta'$ and $K\beta''$ satellites on the low- and high-energy sides of the $K\beta_{1,3}$ peak position, respectively, as explained in the case of copper [4,5]. These satellite lines have also been investigated until now both experimentally and theoretically [1,6,18,21–26] for all $3d$ transition metals. Shake-off from the $3d$ shell was also shown to account reasonably well for the measured $K\beta_{1,3}$ line shape, although a complete quantitative fitting has not been reported, and possible contributions from other shells were not investigated [21,24,25]. More recently, Ito *et al.* [27] measured systematically the $K\beta$ x-ray spectra of the elements from Ca to Ge, using a high-resolution antiparallel double-crystal x-ray spectrometer. They reported that each $K\beta_{1,3}$ natural linewidth has been corrected using the instrumental function of this type of x-ray spectrometer, the spin doublet energies have been obtained from the peak position values in $K\beta_{1,3}$ x-ray spectra, and the contributions of satellite lines were considered to be originated from $[KM]$ shake processes.

In order to elucidate the influence of the shake processes on the spectral profile, we investigated in this paper the contribution of $[1s3d]$ shake-off to the asymmetry of Se, Y, and Zr $K\alpha_{1,2}$ emission lines, from both experiment and theory, and the natural width of each line in the $K\beta_{1,3}$ emission spectra of the same elements to obtain the energy values of the spin doublet in detail, using a high-resolution double-crystal x-ray spectrometer.

II. EXPERIMENTAL METHODOLOGY

In the present paper we used a RIGAKU (3580E) double-crystal x-ray spectrometer. The experimental conditions for the measurements are given in Table I. Using Bragg reflections with this spectrometer, the true FWHM of the emission

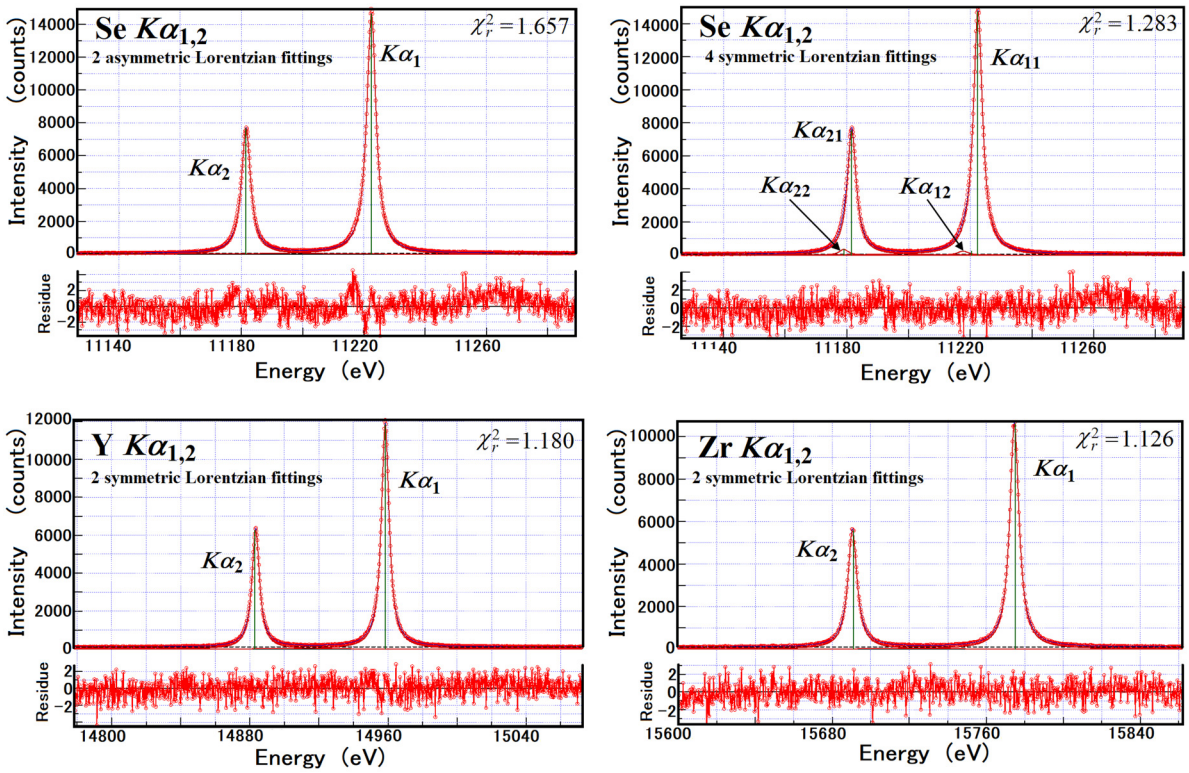

FIG. 1. The observed $K\alpha_{1,2}$ spectra in elements Se, Y, and Zr are shown with the Lorentzian functions used in the fitting processes [20,27]. These spectra were measured using the antiparallel double-crystal x-ray spectrometer described in the text. For Se, on the left side is shown the result of a two-asymmetric Lorentzian fitting analysis, and on the right side the result of a four-symmetric Lorentzian fitting analysis, according to Ito *et al.* [20]. In this figure, $K\alpha_{11}$ is the $K\alpha_1$ diagram line, and $K\alpha_{21}$ is the $K\alpha_2$ line, whereas $K\alpha_{12}$ and $K\alpha_{22}$ are the corresponding satellite lines. The ratio of the $K\alpha_{12}$ to $K\alpha_{11}$ line intensities is used in Fig. 9. The spectra of Y and Zr were analyzed by a two-symmetric Lorentzian fitting. A single scan of three repeat measurements is shown in each element. Each χ_r^2 is a value in a single scan measurement. See the text for details.

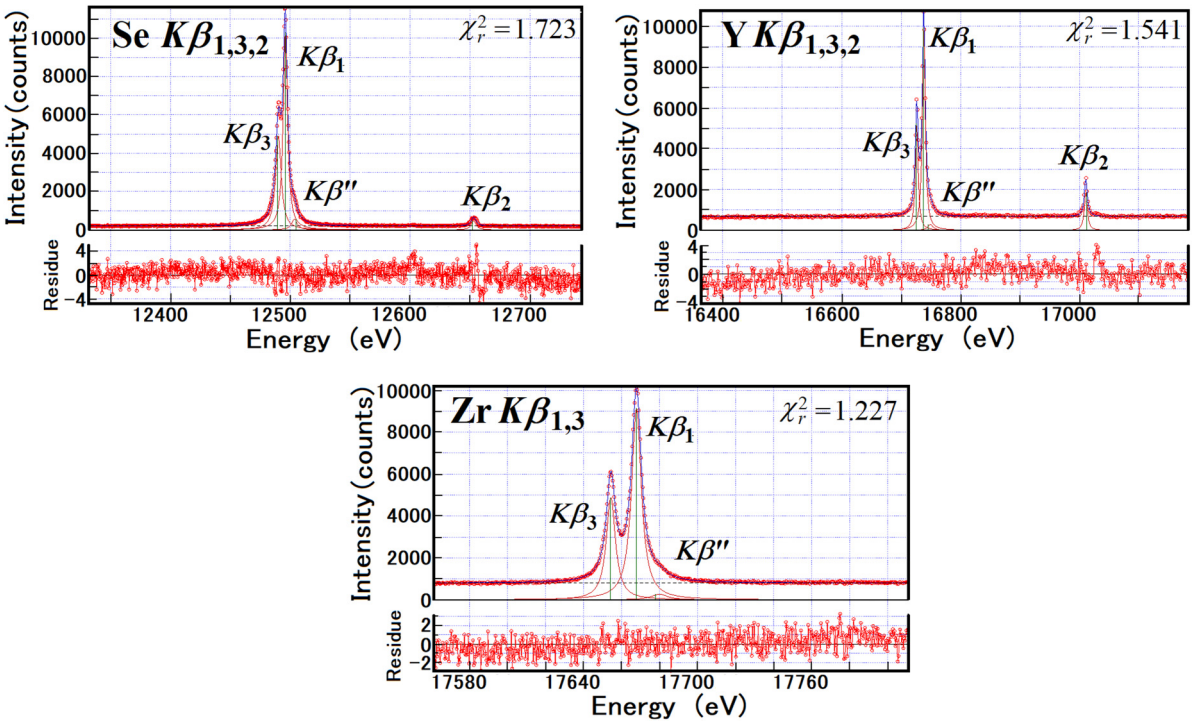

FIG. 2. The observed $K\beta_{1,3}$ spectra in elements Se, Y, and Zr are shown with the fitting Lorentzian functions. These spectra were measured using the antiparallel double-crystal x-ray spectrometer described in detail in Ref. [20,27]. $K\beta''$ are satellite lines on the high energy side of the $K\beta_{1,3}$ spectra. A single scan of three repeat measurements is shown for each element together with the value of χ_r^2.

line can be determined by a simple subtraction of the convolution in the crystal dispersion from the FWHM of the measured emission line [28] (see Refs. [20,27] for details). With a Rh end-window x-ray generator operating at 40 kV and 60 mA, the emitted $K\alpha$ and $K\beta$ spectra (see Figs. 1 and 2) were recorded under a vacuum with a sealed Xe gas proportional counter in the symmetric Si(220) Bragg reflection of the double-crystal spectrometer at an angular step of 0.0005° in 2θ for $K\alpha$ spectra, 0.001° for Se, 0.0025° for Y, and 0.0005° for Zr in 2θ for $K\beta$ spectra. The slits vertical divergence is 0.573° in this spectrometer. Temperature in the x-ray spectrometer chamber is controlled within 35.0 ± 0.5 °C. Acquisition time was 7–120 s/point (see Table I). Neither smoothing nor correction were applied to the raw data. Each spectrum was repeated three times. The energy values of Bearden [29] were taken as starting points for the diagram line fitting parameters. We used metal powder (99.9%, Nacalai Tesque) for Se, metal plate (99%, Nilaco Corporation) for Y, and metal foil (99.2%, Nilaco Corporation) for Zr. The powder Se was confirmed to be the metallic form using a x-ray diffractometer and the double-crystal x-ray spectrometer.

The instrumental function of the double-crystal spectrometer can be very well described from Monte Carlo simulations as has been shown in Refs. [30–32] and by simply computing the rocking curve of the Si crystals through dynamical diffraction theory [33]. From these instrumental functions one can obtain the natural linewidths as well as some other broadening mechanisms. In the present case, given the large natural widths of the diagram lines of neutral atoms when compared to the spectrometer instrumental function, we can use the simple broadening method described by Tochio *et al.* [28] without increasing the final uncertainty.

III. THEORETICAL CALCULATIONS

The level energies, transition amplitudes, and shake probabilities needed to calculate the diagram, and satellite x-ray emission spectra were computed with the relativistic atomic structure code MCDFGME, developed by Desclaux [34] and Indelicato and Desclaux [35]. This code fully implements the multiconfiguration Dirac-Fock (MCDF) method but, in the present calculations, the electronic correlation was only included up to the level of the configuration mixing, and not at the level of a multiconfiguration calculation.

A. Basics of the MCDF method

The N-electron atomic system in the MCDF method is described by the Dirac-Coulomb-Breit (DCB) Hamiltonian,

$$H_{\rm DCB} = \sum_{a=1}^{N} h_a^{\rm D} + \sum_{a=1}^{N-1} \sum_{b=a+1}^{N} V_{ab}^{\rm CB}, \tag{1}$$

where $h_a^{\rm D}$ is the one-electron Dirac Hamiltonian,

$$h_a^{\rm D} = c\boldsymbol{\alpha}_a \cdot \boldsymbol{p}_a + c^2(\beta_a - 1) + V_a^{\rm N}. \tag{2}$$

Here $\boldsymbol{\alpha}_a$ and β_a are the 4×4 Dirac matrices and $V_a^{\rm N}$ describes the interaction of one electron with the atomic nucleus. In the length gauge, the two-electron interaction can be writ-

ten as

$$V_{ab}^{\mathrm{CB}} = \frac{1}{r_{ab}} - \frac{\boldsymbol{\alpha}_a \cdot \boldsymbol{\alpha}_b}{r_{ab}} \cos(\omega_{ab} r_{ab}) + (\boldsymbol{\alpha}_a \cdot \nabla_a)(\boldsymbol{\alpha}_b \cdot \nabla_b) \frac{\cos(\omega_{ab} r_{ab}) - 1}{\omega_{ab}^2 r_{ab}}, \quad (3)$$

where r_{ab} is the interelectrons distance and ω_{ab} is the energy of the exchanged photon between the two electrons. The first term $1/r_{ab}$ describes the instantaneous Coulomb interaction and the remaining terms are known as the Breit interaction. In the limit $\omega_{ab} r_{ab} \ll 1$, the Breit interaction becomes

$$V_{ab}^{\mathrm{B}} \approx -\frac{\boldsymbol{\alpha}_a \cdot \boldsymbol{\alpha}_b}{r_{ab}} - \frac{1}{2}(\boldsymbol{\alpha}_a \cdot \nabla_a)(\alpha_b \cdot \nabla_b) r_{ab}. \quad (4)$$

The first term in this relation is known as the magnetic (Gaunt) interaction, and the second term is the lowest-order retardation interaction, which are calculated in the MCDFGME code as part of the self-consistent variational method. The remaining Breit retardation terms in Eq. (3) were also included perturbatively. Furthermore, the code also accounts for radiative corrections, namely, self-energy and vacuum polarization. For details on the theory QED corrections in atomic systems, we refer the reader to Ref. [36].

The atomic wave functions are calculated in the framework of the variational principle using energy eigenfunctions that are written as linear combinations of configuration state functions (CSF). The CSF are expressed as linear combinations of Slater determinants with the same parity and are eigenfunctions of the Hamiltonian, total angular momentum, and projection of the total angular momentum on the quantization axis of the atomic system. All energy levels for one- and two-hole configurations were calculated with complete relaxation, meaning that both the mixing coefficients and the radial orbitals in the CSF were optimized in the variational method.

B. Calculation of the line intensities

Radiative transition amplitudes were calculated between levels of the K-shell one-hole configurations with full relaxation, that is, initial and final bound-state wave functions were optimized independently. This so-called optimal levels scheme does not ensure the orthogonality of the initial- and final-state spin orbitals. To deal with the nonorthogonality of the wave functions, the code uses the formalism prescribed by Löwdin [37]. Radiationless transition amplitudes were calculated between initial levels of K-shell one-hole configurations and final levels of bound two-hole configurations and an electron in the continuum. The initial levels wave functions were also obtained from the previous energy calculations, but to ensure orthogonality, no orbital relaxation was allowed between the initial and the final bound-state wave functions. Nonetheless, the radiationless rates were calculated using the more accurate transition energies obtained in the first step.

From the results of these calculations, we computed all diagram line intensities from initial levels i to all possible final levels f where the indices i and f stand for the electronic configurations C_i and C_f, the total angular momenta J_i and J_f, respectively, and all other quantum numbers required to completely specify these levels,

$$I_{\mathrm{if}} = N_i E_{\mathrm{if}} B_{\mathrm{if}} \omega_i. \quad (5)$$

Here, N_i is the population of level i, $E_{\mathrm{if}} = E_i - E_f$ is the transition energy, B_{if} is the x-ray emission branching ratio,

$$B_{\mathrm{if}} = \frac{A_{\mathrm{if}}^{\mathrm{R}}}{\sum_{f'} A_{\mathrm{if}'}^{\mathrm{R}}} = \frac{A_{\mathrm{if}}^{\mathrm{R}}}{A_i^{\mathrm{R}}}, \quad (6)$$

and ω_i is the initial level fluorescence yield,

$$\omega_i = \frac{A_i^{\mathrm{R}}}{A_i^{\mathrm{R}} + A_i^{\mathrm{NR}}} = \frac{\sum_{f'} A_{\mathrm{if}'}^{\mathrm{R}}}{\sum_{f'} A_{\mathrm{if}'}^{\mathrm{R}} + \sum_{f''} A_{\mathrm{if}''}^{\mathrm{NR}}}, \quad (7)$$

where $A_{\mathrm{if}'}^{\mathrm{R}}$ and $A_{\mathrm{if}''}^{\mathrm{NR}}$ are the radiative and radiationless transition amplitudes, respectively, between two levels. In Eqs. (6) and (7), f' and f'' stand for all possible levels that can be reached from level i by radiative and radiationless transitions, respectively. The populations of levels i are taken to be statistical, which means that all states of the initial levels of a given configuration have the same probability of being populated

$$N_i = \frac{(2J_i + 1)}{\sum_{i'}(2J_{i'} + 1)}, \quad (8)$$

where the summation runs over all levels belonging to configuration C_i.

The radiative transition amplitudes in the length gauge can be written as the Einstein A coefficients for the photon emission,

$$A_{\mathrm{if}}^{\mathrm{R}} = \frac{2(J+1)(2J+1)}{J\{[(2J+1)!!]^2\}} \left(\frac{E_{\mathrm{if}}}{\hbar c}\right)^{2J+1} \frac{|\langle f||Q_J||i\rangle|^2}{2J_i + 1}, \quad (9)$$

where Q_J are the many-electron multipole transition operators of rank J as defined in Ref. [38]. All electric and magnetic multipole transitions with $J \leqslant 3$ were included in the present calculations. The radiationless transition amplitudes were calculated assuming the sudden approximation using perturbation theory. The calculation was performed in the frozen-core approximation, including both direct and exchange terms [39].

Satellite lines correspond to transitions where a second "spectator" hole is present and occur when initial double-hole levels exist. This double ionization may result from shake-off, that is, the ejection of an outer electron due to the sudden change in nuclear potential when an inner hole is created. This process was considered by Bloch [40] and used for the first time by and Demekhin and Sachenko [41] to calculate for the first time shake satellite intensities in the x-ray spectra. Åberg [42] also used the sudden approximation for the calculation of $K\alpha_1\alpha_2$ satellite line intensities in Ne-like ions. Frequently, the number of satellite lines is so large that they are seen in the spectra as bands as in the present spectra.

To compute satellite branching ratios, we used radiative transition amplitudes between levels of two-hole configurations, calculated in the same way as for the one-hole configurations but limited to $J \leqslant 1$. An exact calculation of satellite intensities also requires the calculation of radiationless transition amplitudes between initial two-hole and final three-hole configuration levels to obtain the satellite level fluorescence yield $\omega_{i'}^{\mathrm{sat}}$. This, however, would be computationally

TABLE II. Number of K-shell transitions involved in the calculations presented in this paper. Radiationless and satellite transitions are grouped in final two-hole configurations $[KX\ [L1X], \ldots [O1X],\ [L3X], \ldots$, where $X = K, L1, O1$.

Element	Se	Y	Zr	Element	Se	Y	Zr	Element	Se	Y	Zr
Transition		Radiative		Transition		Radiationless		Transition		Satellite	
								KK-KX	596	210	2372
*K-L*1	64	14	244	*K-L*1*X*	1496	792	8208	*KL*1-*L*1*X*	2004	735	8596
*K-L*2	64	7	244	*K-L*2*X*	1368	484	7676	*KL*2-*L*2*X*	1995	740	8574
*K-L*3	104	29	433	*K-L*3*X*	2112	765	12975	*KL*3-*L*3*X*	5033	2080	26614
*K-M*1	64	14	244	*K-M*1*X*	1032	396	6256	*KM*1-*M*1*X*	2003	737	8598
*K-M*2	64	14	244	*K-M*2*X*	888	368	5904	*KM*2-*M*2*X*	2006	747	8743
*K-M*3	104	22	433	*K-M*3*X*	1344	580	9215	*KM*3-*M*3*X*	5004	2052	26335
*K-M*4	112	22	433	*K-M*4*X*	984	484	8028	*KM*4-*M*4*X*	5076	2153	28366
*K-M*5	106	23	539	*K-M*5*X*	656	448	7152	*KM*5-*M*5*X*	6328	2816	40697
*K-N*1	64	14	244	*K-N*1*X*	120	136	2160	*KN*1-*N*1*X*	2004	735	8594
*K-K*2	40	14	214	*K-N*2*X*	32	97	1567	*KN*2-*N*2*X*	857	715	5576
*K-N*3		22	465	*K-N*3*X*	8	100	1839	*KN*3-*N*3*X*		2113	33461
*K-N*4		1	32	*K-N*4*X*		4	80	*KN*4-*N*4*X*		11	212
*K-O*1		14	244	*K-O*1*X*		8	144	*KO*1-*O*1*X*		735	8597
Total	786	210	4013	Total	10040	4662	71204	Total	32906	16579	215335

very demanding and, instead, we approximated the fluorescence yield of the satellite-line initial level by the K-shell fluorescence yield,

$$\omega_{i'}^{\mathrm{sat}} \approx \omega_K = \frac{\sum_i A_i^{\mathrm{R}}}{\sum_i \left(A_i^{\mathrm{R}} + A_i^{\mathrm{NR}}\right)}, \tag{10}$$

where i' labels the satellite level belonging to a $[KX]$ ($X = K, L, M, \ldots$) two-hole configuration.

The calculation of the satellite intensities was performed using the expression equivalent to Eq. (5) but with each line intensity weighted by the shake-off probability of the initial level. The shake-off probabilities were calculated in the sudden approximation, according to the method of Carlson and Nestor [43], using the overlap integrals between orbitals in the neutral and the one-hole K-shell configurations.

To produce the theoretical spectra, the transition intensities distribution was convoluted with a line-shape function that accounted for the natural and experimental broadening. The line-shape function consisted of two Lorentzian with different widths: the natural width, calculated from the partial sum of radiative and radiationless amplitudes, and the experimental width. The choice of two Lorentzian is based on the fact that the rocking curve of the Si crystals in double-crystal spectrometers resembles much better a Lorentzian than a Gaussian profile.

The number of transitions calculated in this paper is shown in Table II. The simulations of the $K\alpha_{1,2}$ and $K\beta_{1,3}$ lines of Se, Y, and Zr, as well as the corresponding resulting satellite bands can be seen in Fig. 3 together with the experimental plots. In Fig. 4 are presented, as an example, the individual satellite bands due to shake-off from the different orbitals for Y, and the resulting overall satellite band. In Table V we list the probabilities (in percentages) of shake processes as the result of a sudden 1s vacancy production for all shells.

Thus, our spectra calculations are fully *ab initio* without resorting to any kind of fit other than the energy offset of all transitions due to the lack in the calculations of physical effects, such as Auger shifts and small corrections due to higher-order multiconfiguration electronic correlation. The values of the energy offset that were obtained by fitting the final theoretical spectral shape (satellites included) to the experimental data are (in eV) 1.15 ± 0.05 for Se $K\alpha$, 1.90 ± 0.05 for Se $K\beta$, 1.50 ± 0.05 for Y $K\alpha$, 3.50 ± 0.05 for Y $K\beta$, 1.55 ± 0.05 for Zr $K\alpha$, and 4.15 ± 0.05 for Zr $K\beta$ and are the same for each line component, either diagram or satellite, meaning that within each plot of Figs. 3 and 4 there is only one global energy offset. The same occurs for the intensity offset, which is just a constant for each plot.

The use of the multi-Lorentzian fitting for diagram and satellite lines, although not strictly valid, serves the purpose of allowing the comparison with a common framework used extensively by experimentalists in the x-ray emission spectrometry field. As can be seen in Fig. 4, the shape of the satellite bands cannot be truly fitted by a single Lorentzian, however, it is remarkable that for the $K\alpha$ lines of Se, the inclusion of only one Lorentzian for each diagram and satellite line results in such a low χ_r^2 (see Fig. 1).

IV. RESULTS AND DISCUSSION

As described in Sec. I, asymmetric line shapes in x-ray emission spectra were attributed as early as 1927 to the existence of one-electron transitions in the presence of a spectator hole, resulting from shake processes after ionization by photons, electrons, and other particles [1,6,7]. After Deutsch *et al.* [4] demonstrated that the line profiles of Cu $K\alpha$ and $K\beta$ emission lines can be fully accounted for by contributions to the diagram lines from 3d-spectator transitions only, Hölzer *et al.* [6] concentrated on the investigation of $K\alpha$ and $K\beta$ diagram lines based on the results of Deutsch *et al.* [4] in order to elucidate the origin of the asymmetry using a high-resolution x-ray crystal spectrometer.

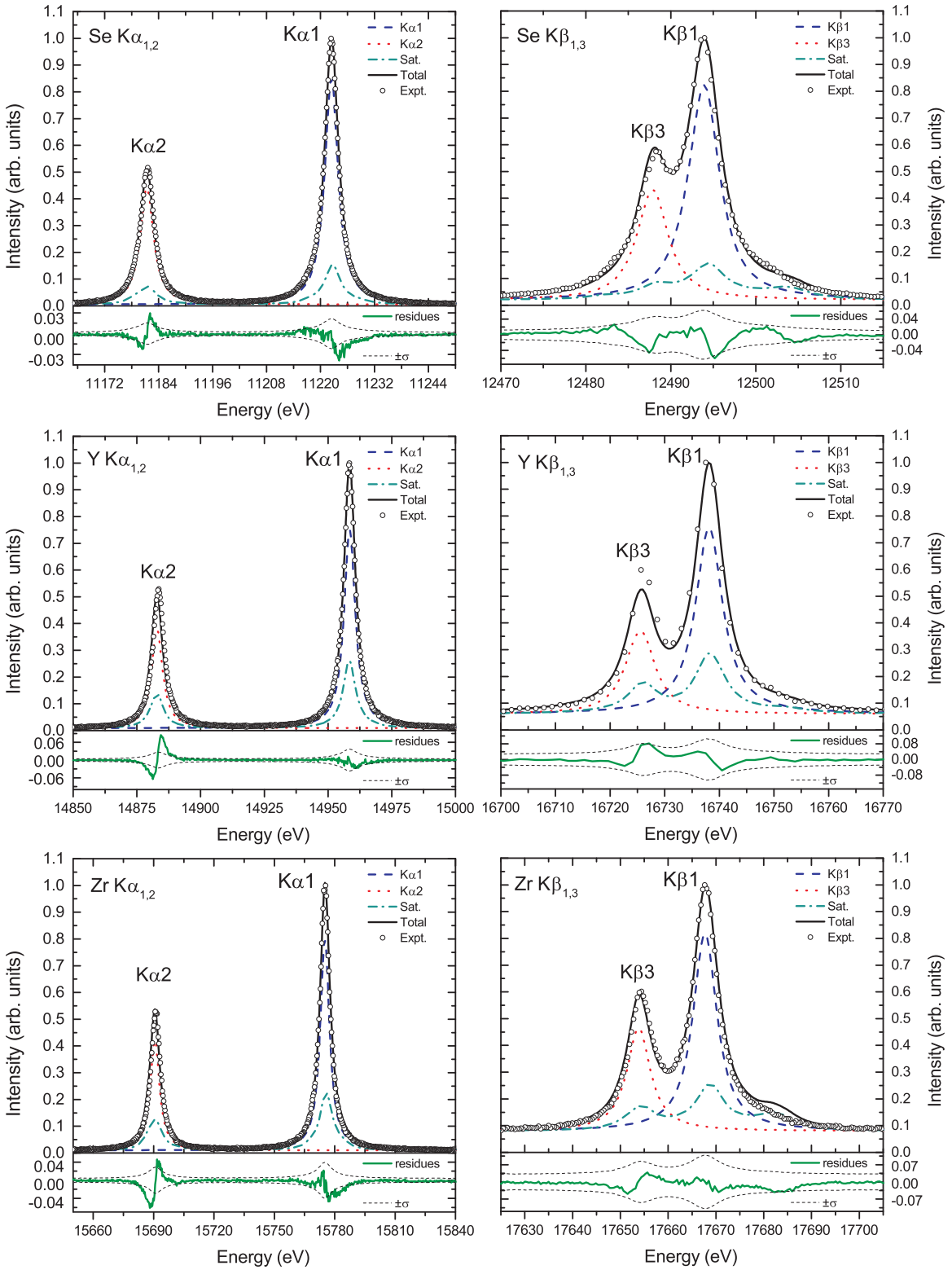

FIG. 3. Simulation of the $K\alpha_{1,2}$ and $K\beta_{1,3}$ lines of Se, Y, and Zr, together with the experimental data. Both diagram and satellite lines account for the final line shape. The curves labeled "Sat." are the sum of all satellite lines.

According to Hölzer *et al.* [6], only few of the previous data were corrected for instrumental broadening, although it was realized early that broadening from this origin has a significant effect [44]. A two-flat-crystal x-ray spectrometer, using a crystal instead of the slit in a single-flat-crystal x-ray spectrometer, is used for our studies. This spectrometer was developed by Gohshi *et al.* [45] with the two crystals linked. Tochio *et al.* [28] evaluated the instrumental broadening in this type spectrometer. Ito *et al.* [20] investigated systematically the asymmetry index, FWHM, and intensity

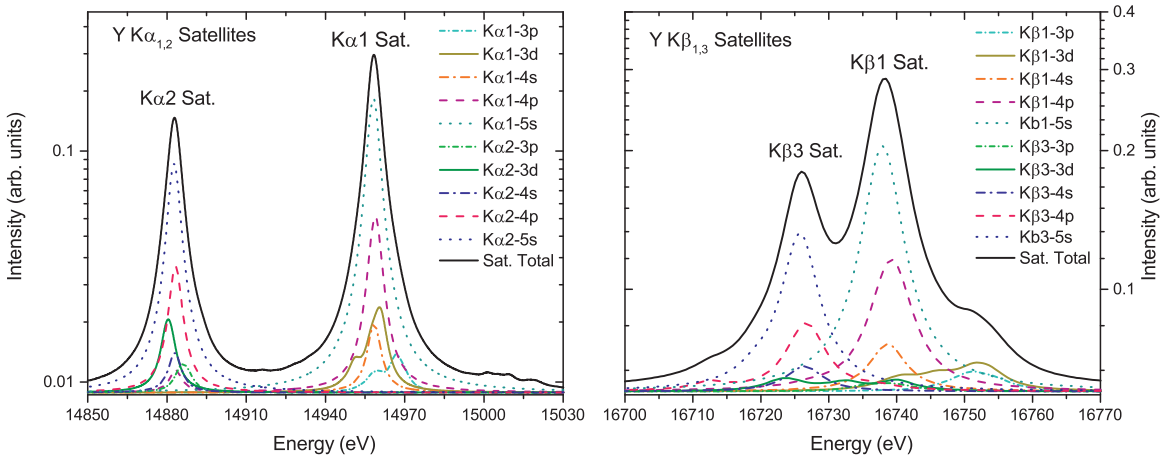

FIG. 4. Simulation of the $K\alpha_{1,2}$ and $K\beta_{1,3}$ satellite lines of Y. The resulting satellite band is represented, together with the components resulting from shake-off from the individual orbitals. In order to better identify the individual satellites, the ordinate is shown in logarithmic scale and only the most intense curves are shown. The small structure on the high-energy side of the $K\alpha_{1,2}$ spectrum is due to $2p$ spectator holes.

ratio of $K\alpha_{1,2}$ diagram lines in $3d$ transition elements using the double-crystal x-ray spectrometer in order to elucidate the origin of the asymmetry in the line profile. They showed that the asymmetry index of $K\alpha_1$ in the elements from Sc to Ge is ascribed to the existence of a $3d$ spectator hole. In which element the asymmetry of $K\alpha$ lines appears was discussed.

In the present paper, the $K\alpha_{1,2}$ and $K\beta_{1,3}$ spectra of elements Se, Y, and Zr, have been measured three times each, using a high-resolution double-flat-crystal x-ray spectrometer. The values of the obtained averaged line energies and averaged relative intensity ratios for each line in each Lorentzian model for these elements are shown in Tables III and IV, respectively. The corrected FWHM for the $K\alpha_{1,2}$ and $K\beta_{1,3}$ diagram lines are presented in Tables III and IV, and Figs. 5–8, respectively, together with values reported by other authors [46,47]. The corrected FWHM values were taken from the observed FWHM through the method of Tochio *et al.* [28].

A. The observed $K\alpha_{1,2}$ emission spectra

The two-asymmetric and the four-symmetric Lorentzian fittings are performed only for Se. The two-symmetric Lorentzian fittings are performed also for Y and Zr. This is because the contribution of the $[1s3d]$ shake process could not be clearly confirmed from the observed spectra through the fitting method as seen in Fig. 1. The asymmetry index is defined as the ratio of the half width at half maximum

TABLE III. The observed $K\alpha_{1,2}$ spectra in elements Se, Y, and Zr are shown with the Lorentzian functions used in the fitting processes [4,20]. $K\alpha_{11}$ spectra are the $K\alpha_1$ diagram line, and $K\alpha_{21}$ spectra are the $K\alpha_2$ diagram line. $K\alpha_{12}$ and $K\alpha_{22}$ satellite lines are due to the shake processes. The corrected FWHM was obtained by the method of Tochio *et al.* [28]. All energy values are in eV. The values of the instrumental broadening are around 0.17, 0.21, and 0.22 eV for Se, Y, and Zr $K\alpha_1$ photon energy, respectively. The asymmetry index is defined as the ratio of the half width at half maximum on the low- and high-energy sides of each peak, respectively.

Element/lines	Energy	FWHM	Corrected FWHM	Ref. [46]	Ref. [47]	Asymetry index	I_{rel} (%)
Se	Two-asymmetric Lorentzian						
$K\alpha_1$	11222.383(94)	3.727(15)				1.028(9)	100
$K\alpha_2$	11181.439(96)	3.689(23)				1.028(11)	51.78(20)
Se	Four-symmetric Lorentzian						
$K\alpha_{11}$	11222.380(89)	3.633(20)	3.468(20)	3.3	3.33		100
$K\alpha_{12}$	11217.573(65)	3.53(80)					1.68(52)
$K\alpha_{21}$	11181.48(10)	3.579(39)	3.414(39)	3.33	3.46		50.83(64)
$K\alpha_{22}$	11178.55(41)	3.02(76)					1.80(88)
Y	Two-symmetric Lorentzian						
$K\alpha_1$	14958.389(24)	5.464(27)	5.254(27)	4.94	5.02		100
$K\alpha_2$	14883.403(39)	5.393(40)	5.216(40)	5.04	5.18		52.23(23)
Zr	Two-symmetric Lorentzian						
$K\alpha_1$	15774.87(31)	5.865(31)	5.645(31)	5.34	5.4		100
$K\alpha_2$	15690.77(30)	5.845(44)	5.625(44)	5.46	5.62		52.53(27)

TABLE IV. The observed $K\beta_{1,3}$ spectra in elements Se, Y, and Zr are shown with the Lorentzian functions used in the fitting process [27]. $K\beta''$ spectra are satellite lines (see Ref. [4,5,27] and references therein). The fitting analyses in Se, Y, and Zr were executed with symmetric Lorentzians. The corrected FWHM was obtained by the method of Tochio *et al.* [28]. All energy values are in eV.

Element/lines	Energy	FWHM	Corrected FWHM	Ref. [46]	I_{rel} (%)
Se	Symmetric Lorentzian				
$K\beta_1$	12495.911(26)	4.285(87)	4.085(87)	4.48	100
$K\beta_3$	12490.094(44)	5.70(10)	5.50(10)	4.48	63.3(1.1)
$K\beta''$	12503.11(30)	6.25(71)			8.1(1.3)
$K\beta_2$	12652.840(77)	4.81(24)			5.24(34)
Y	Symmetric Lorentzian				
$K\beta_1$	16737.88(29)	5.60(25)	5.38(25)	5.46	100
$K\beta_3$	16726.02(28)	5.53(17)	5.31(17)	5.46	52.6(1.8)
$K\beta''$	16746.2(2.9)	17.0(6.1)			1.80(88)
$K\beta_2$	17010.57(16)	5.80(25)			1.68(52)
Zr	Symmetric Lorentzian				
$K\beta_1$	17667.78(30)	6.171(88)	5.791(88)	5.83	100
$K\beta_3$	17654.31(23)	5.89(10)	5.51(10)	5.83	50.49(60)
$K\beta''$	15774.87(31)	10.8(1.7)			5.2(1.3)

on the low- and high-energy sides of each peak, respectively, providing a measure of the peak asymmetry [49].

The corrected FWHM of the $K\alpha_1(K\alpha_{11})$ and $K\alpha_2(K\alpha_{21})$ diagram lines, additionally corrected for the instrumental broadening, are presented in Figs. 5 and 6 together with the recommended values based on experimental results of Campbell and Papp [46] and the semiempirical values of Krause and Oliver [47] (when fitting $K\alpha_{1,2}$ spectral lines with four Lorentz functions in 3*d* elements, the ones corresponding to the two diagram lines, that is, $K\alpha_{11}$ and $K\alpha_{21}$, are shown).

For Se, the values of the obtained averaged line energies, averaged FWHM, averaged asymmetry indexes, and averaged relative intensity ratios for each line in the asymmetric model are given in Table III, and averaged line energies, averaged observed FWHM, averaged corrected FWHM, and averaged relative intensity ratio in four symmetric Lorentzian model are also shown in Table III. The instrumental broadening was found to be 0.17, 0.21, and 0.22 eV of $K\alpha_1$ in Se, Y, and Zr, respectively, using the method of Tochio *et al.* mentioned above, and the CFWHMs were obtained by subtraction from the FWHMs. Moreover, for Y and Zr, the values of the obtained averaged line energies, averaged FWHM, averaged corrected FWHM, and averaged relative intensity ratio in $K\alpha_1$ and $K\alpha_2$ lines, in each symmetric Lorentzian model are shown in Table III as well as the other reported data, that is, Krause

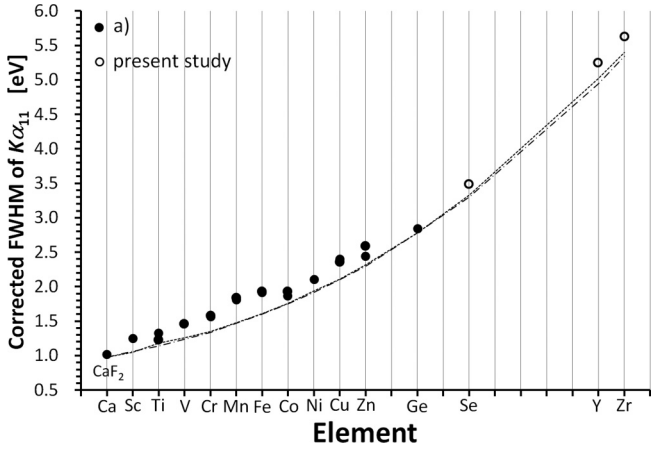

FIG. 5. The corrected FWHM of the $K\alpha_1$ line of elements Se, Y, and Zr are shown, together with the semiempirical values reported by Krause and Oliver [47], and the recommended values, based on experimental results, of Campbell and Papp [46]. The values of Krause and Oliver are represented by the dotted line and those reported by Campbell and Papp by the dots and dashed line. The data (a) from Ito *et al.* [20] were used for only Si(220) analyzing crystals in a vacuum. The corrected FWHM values for the $K\alpha_1$ diagram lines in the elements Se, Y, and Zr were obtained from the observed FWHM through the method of Tochio *et al.* [28]

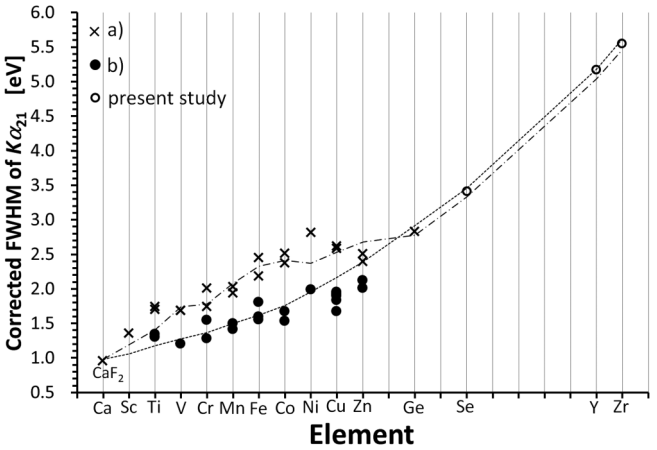

FIG. 6. The corrected FWHM of the $K\alpha_2$ line of elements Se, Y, and Zr are shown together with the semiempirical values reported by Krause and Oliver [47] marked by dotted line, and the recommended values of Campbell and Papp [46] marked by dotted and dashed line. Solid circles in (b) are the values subtracting the Coster-Kronig broadening effects reported by Ito *et al.* [20]. Crosses in (a) are from the observed data of $K\alpha_2$ in Ref. [20]. The corrected FWHM values for the $K\alpha_2$ diagram line in the elements Se, Y, and Zr were obtained from the observed FWHM through the method of Tochio *et al.* [28].

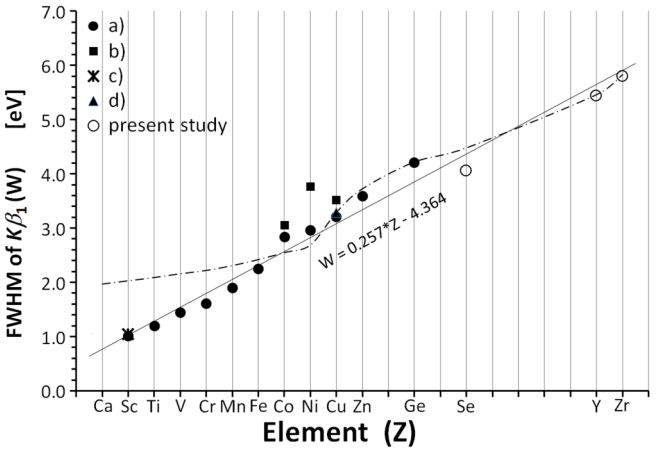

FIG. 7. The corrected FWHM of the $K\beta_1$ line of elements Se, Y, and Zr together with the recommended values reported by Campbell and Papp [46] marked by dots and dashed curve. The linear function W is obtained by the least-squares method using $K\beta_1$ linewidths [27]. (a) Ito *et al.* [27]. (b) Hölzer *et al.* [6]. (c) Anagnostopolos *et al.* [18]. (d) Pham *et al.* [26].

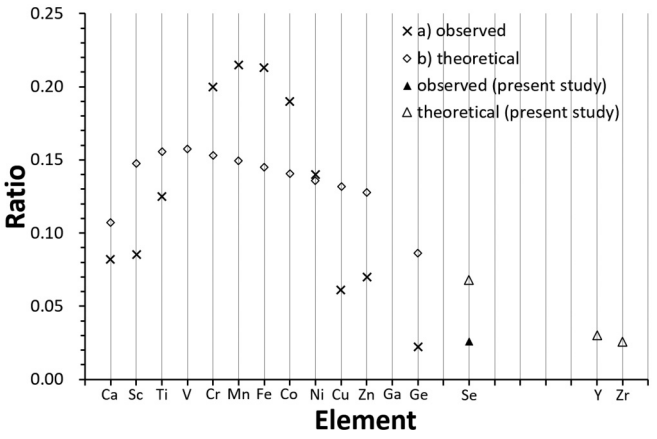

FIG. 9. Ratio of $K\alpha_{12}$ satellite to the $K\alpha_{11}$ diagram line intensities in Se is shown by a black triangle together with those of Refs. [20,48] marked by crosses (a). According to Ito *et al.* [20], this satellite is mainly considered to be a contribution of the $[1s3d]$ shake process to the asymmetry of the $K\alpha_1$ emission line. Open rhombohedra (b) from Ref. [20] and open triangles from Table V represent the shake probability of $[KM]$, respectively. These values are based on the theoretical calculations. See the text in details.

and Oliver semiempirical natural linewidths [47], and the recommended linewidth values of Campbell and Papp [46].

We checked the Cu $K\alpha_{1,2}$ diagram lines as standard lines in order to evaluate the reproducibility in the double-crystal x-ray spectrometer, whereas measuring the $K\alpha_{1,2}$ and $K\beta_{1,3}$ diagram lines for each element [20,50]. The fitting process with the Lorentzian functions shown in Fig. 1 for $K\alpha_{1,2}$ and Fig. 2 for $K\beta_{1,3}$ diagram lines, used the procedure provided in IGOR PRO (HULINKS, Inc.) software application. The values of χ_r^2 are shown in these figures. In our case, N in χ_r^2 is the number of the fitted data points. In the fitting process no constraints have been imposed. Moreover, Figs. 1 and 2 show a single scan of three repeat measurements in each element. The errors quoted in Table III are, thus, only statistical errors resulting from the fitting processes and the limited reproducibility of the experimental setup. To obtain realistic uncertainties, the errors originating from the energy calibration have to be considered. Absolute $K\alpha_{1,2}$ and $K\beta_{1,3}$ photon energies for all $3d$ elements between Cr and Cu can be found in Ref. [6].

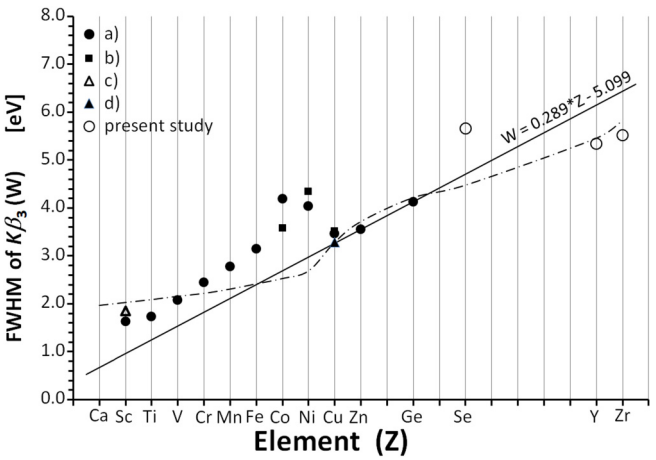

FIG. 8. The corrected FWHM of the $K\beta_3$ line of elements Se, Y, and Zr is shown together with the recommended values [46].The linear function W was obtained by the least-squares method using $K\beta_1$ linewidths in the elements Zn and Ge [27]. (a) Ito *et al.* [27]. (b) Hölzer *et al.* [6]. (c) Anagnostopoulos *et al.* [18]. (d) Pham *et al.* [26].

In Figs. 5 and 6 we can see that the overall variation behavior with Z of the $K\alpha_{11}$ (or $K\alpha_1$) and $K\alpha_{21}$ (or $K\alpha_2$) lines is well reproduced by the data reported by Campbell and Papp [46] and Krause and Oliver [47]. We obtained the corrected FWHM values for both $K\alpha_{11}$ (or $K\alpha_1$) and $K\alpha_{21}$ (or $K\alpha_2$) diagram lines from the observed FWHM through the method of Tochio *et al.* [28]. Ito *et al.* [20] attributed the difference in $K\alpha_{11}$ and $K\alpha_{21}$ diagram lines corrected FWHM values observed in $3d$ elements to the broadening effect of the Coster-Kronig transitions.

In what concerns the asymmetry of the $K\alpha_1$ diagram line, Ito *et al.* [20] concluded that it is due to the $[1s3d]$ shake processes as seen in Fig. 9. Through precise experiments and theoretical considerations, we investigated up to which elements the influence of the $[1s3d]$ shake processes contributes to the $K\alpha_1$ emission spectrum. In Table V and Fig. 9 (shake probability ratio), the $[KX]$ $(X = M, N, O)$ shake probabilities are shown for Se, Y, and Zr. The $[1s3d]$ shake probability is relatively large, at least, until element Zr. However, an asymmetric $K\alpha_1$ profile can be observed for Se, whereas in Y and Zr it is very difficult to distinguish the satellite lines from the diagram lines. One should consider that the shake probabilities of $[KN]$ or $[KO]$ hidden satellites are large in these elements as seen in Table V. Therefore, it is hard to discuss the asymmetry in the $K\alpha_1$ spectra of elements with atomic numbers larger than Y based on both the experimental results and the theoretical calculations of the shake process as seen in Figs. 1 and 3 because, according to Ito *et al.* [20], the asymmetry depends on the $[KM]$ shake probability and

TABLE V. Probabilities (in percentages) of shake processes for various shells as the result of a sudden 1s vacancy production.

	Se ($Z = 34$)	Y ($Z = 39$)	Zr ($Z = 40$)
$1s$	0.0045	0.0034	0.0032
$2s$	0.0620	0.0417	0.0403
$2p_{1/2}$	0.1080	0.0738	0.0690
$2p_{3/2}$	0.2110	0.1408	0.1313
$3s$	0.2670	0.1705	0.1623
$3p_{1/2}$	0.5060	0.3178	0.2949
$3p_{3/2}$	1.1090	0.6188	0.5731
$3d_{3/2}$	1.9230	0.8201	0.7182
$3d_{5/2}$	2.8700	1.0537	0.8979
$4s$	3.1080	1.6582	1.4925
$4p_{1/2}$	6.5250	2.1367	1.7826
$4p_{3/2}$	8.2610	4.2805	3.5548
$5s$		14.6472	12.8722
$4d_{3/2}$		7.3547	7.8592
$4d_{5/2}$			1.1906

for elements higher than Y, the influence of the shake process due to $[KN]$ and $[KO]$ becomes larger than the influence of $[KM]$ shake process. It is noteworthy that for these elements the observed spectra are almost symmetrical.

From the theoretical calculations and the simulated line shapes, we conclude that the $[1s3d]$ satellites present themselves as small peaks aligned with the diagram centroid with shoulders on the low-energy side of the diagram line as expected from Fig. 1. Nevertheless, the $[1s3p]$ satellites also contribute to a small asymmetry on the high-energy side of the simulated diagram peaks, although these could not be confirmed experimentally. It may be due to the detection limit of the measurement. This cannot be seen in the $K\alpha$ spectra of all the measured elements but is more pronounced in Zr and, to some extent, Se. Other than that very subtle effect, the *ab initio* simulated $K\alpha$ spectra present a very good agreement with the experimental data (see Fig. 3) both on the overall shape and the intensity ratios.

B. The observed $K\beta_{1,3}$ emission spectra

The values of the obtained averaged line energies and averaged relative intensity ratios for each line of $K\beta_{1,3}$ or $K\beta_2$ in each Lorentzian model for Se, Y, and Zr, are shown in Table IV. The corrected FWHM for the $K\beta_1$ and $K\beta_3$ diagram lines are presented in Table IV, and Figs. 7 and 8, respectively, together with values reported by other authors [6,18,26,27]. The corrected FWHM values were taken from the observed FWHM through the method of Tochio *et al.* [28]. The $K\beta_{1,3}$ spin doublet values observed and calculated in this paper are presented in Table VI and Fig. 10, respectively, together with other observed values [6,18,26,27]. The Lorentzian model was used for an analytic representation of $K\beta$ x-ray lines [27], and the results of the fitting analysis are shown in Fig. 2 for Se, Y, and Zr. The errors quoted in Tables IV and VI are, thus, only statistical errors resulting from the fitting processes and the limited reproducibility of the experimental setup. In Fig. 7, the linear function W shown by a solid line was found by the least-squares method with the corrected FWHM of Sc $K\beta_1$ as an initial value in order to compare with the recommended FWHM of Campbell and Papp [46]. We can see that the overall variation behavior with Z of the corrected FWHM of the $K\beta_1$ line may be linearly fitted with the function $W = 0.257 \times Z - 4.364$ and these values are consistent with those of Ref. [46] marked in dots and dashed line between the elements Fe and Zr. What happens to the change in the corrected FWHM, when the Z number is over 40, has to wait for future research. Furthermore, when the value of Z is less than 26, the corrected FWHM largely deviates from the recommended value. This value is a little different from the function $W = 0.300 \times Z - 5.445$ previously reported [27]. This difference is due to the fact that the $K\beta_1$ linewidths [27] data were evaluated by adding the widths of the Se, Y, and Zr $K\beta_1$ lines. The obtained W values were corrected using the corrected FWHM of $K\beta_1$ lines in the same elements. We consider the obtained linear function W to be more reliable. We will discuss this later.

In Fig. 8, the linear function W, represented by a solid line, was obtained using the corrected FWHMs of Zn and Ge $K\beta_3$ in order to compare with the data of Campbell and Papp [46] because these elements have comparatively small effects of the shake processes $[KM]$ on the diagram lines in $3d$ elements as seen in Fig. 9. The corrected FWHM values of the $K\beta_3$ lines between Cu and Zr, with the exception of Se, are consistent with those of the $K\beta_3$ from Ref. [46], although the corrected FWHM values of the $K\beta_3$ lines in $3d$ elements are very different from those reported therein. The cause of the deviation of the Se $K\beta_3$ line from the linear function W is unknown. The explanation of the tendency of the corrected FWHM of the $K\beta_3$ line is much more difficult than that in the $K\beta_1$ line case. It is necessary to collect experimental data of $K\beta_3$ lines with atomic Z of 40 or more and 20 or less, using this type of x-ray spectrometer in order to elucidate the complexity of the tendency of the corrected FWHM in $K\beta_3$ as a function of Z.

The $K\beta_{1,3}$ spin doublet values observed and calculated in this paper are presented in Table VI together with other reported values [29,46,51] and in Fig. 10 together with other observed values [6,18,26,27]. From the fitting analysis of the $K\beta_{1,3}$ spectra in these elements, the photon energies of the $K\beta_{1,3}$ and $K\beta''$ or $K\beta_2$ lines are presented in Tables IV and VI together with the other reports [29,51] for comparison. The spin doublet energy dependency on the atomic number Z is obtained using the data from Ito *et al.* [27] and the present paper, and the logarithmic function is almost the same as that reported by Ito *et al.* [27], that is, $\log_{10} S = 0.065(Z - 24.879) + 0.149$. However, the physical meaning of this function is not clarified yet.

Now we considered the validity of the logarithmic function of the spin doublet (Fig. 10) in what concerns the $K\beta_1$ and $K\beta_3$ lines (Figs. 7 and 8). The FWHM by fitting analysis of the measured data of Ca $K\beta_{1,3}$ emission lines was obtained in the following way: The double-crystal x-ray spectrometer was used to measure Ca $K\beta_{1,3,5}$ spectra in a $CaCO_3$ compound, using Si(220) analytical crystals. The primary target was tungsten, and the tube voltage and tube current were 40 kV and 70 mA, respectively. The step angle in 2θ was 0.005° and the measuring time was 500 s/point. Ca $K\beta_{1,3}$ spectral lines cannot be separated even by a high-resolution measurement. The

TABLE VI. Comparison of experimental and theoretical K x-ray line energies for Se, Y, and Zr. All energy values are in eV.

		Se ($Z = 34$)	Y ($Z = 39$)	Zr ($Z = 40$)
Present paper	$K\alpha_1$	11222.383(94)	14958.389(24)	15774.87(31)
Experiment	$K\alpha_2$	11181.439(96)	14883.403(39)	15690.77(30)
	$K\alpha_1$-$K\alpha_2$	40.944(4)	74.985(15)	84.109(44)
	$K\alpha_{11}$	11222.380(89)		
	$K\alpha_{21}$	11181.48(10)		
	$K\alpha_{11}$-$K\alpha_{21}$	40.905(15)		
	$K\beta_1$	12495.911(26)	16737.89(29)	17667.78(30)
	$K\beta_3$	12490.094(44)	16726.02(28)	17654.31(23)
	$K\beta_1$-$K\beta_3$	5.817(19)	11.860(51)	13.463(66)
	$K\beta_2$	12652.840(77)	17010.57(16)	
Present paper	$K\alpha_1$	11222.4	14958.3	15774.9
Theory	$K\alpha_2$	11181.6	14883.1	15690.7
	$K\alpha_1$-$K\alpha_2$	40.8	75.2	84.2
	$K\beta_1$	12495.9	16738.5	17667.8
	$K\beta_3$	12490.1	16726.6	17654.2
	$K\beta_1$-$K\beta_3$	5.8	11.9	13.6
	$K\beta_2$	12653.4	17010.5	
Bearden	$K\alpha_1$	11222	14958.8	15775.1
Experiment	$K\alpha_2$	11181.6	14882.9	15690.9
	$K\alpha_1$-$K\alpha_2$	40.4	75.5	84.2
Deslattes	$K\alpha_1$	11222.52(12)	14958.54(27)	15774.914(54)
Experiment	$K\alpha_2$	11181.53(31)	14882.94(26)	15690.645(50)
	$K\alpha_1$-$K\alpha_2$	40.99	75.6	84.269
Deslattes	$K\alpha_1$	11222.55(48)	14958.14(53)	15774.87(54)
Theory	$K\alpha_2$	11181.82(52)	14883.06(58)	15690.61(60)
	$K\alpha_1$-$K\alpha_2$	40.73	75.14	84.26
Bearden	$K\beta_1$	12495.9	16737.8	17667.8
Experiment	$K\beta_3$	12489.6	16725.8	17654
	$K\beta_1$-$K\beta_3$	6.3	12	13.8
	$K\beta_2$	12652.2	17015.4	
Deslattes	$K\beta_1$	12496.03(67)	16738.08(67)	17666.578(76)
Experiment	$K\beta_3$	12489.7(10)	16725.9(10)	17652.628(75)
	$K\beta_1$-$K\beta_3$	6.33	12.18	13.95
	$K\beta_2$	12652.29(96)	17015.6(14)	
Deslattes	$K\beta_1$	12496.5(12)	16738.4(12)	17667.4(12)
Theory	$K\beta_3$	12490.3(12)	16726.8(13)	17654.1(13)
	$K\beta_1$-$K\beta_3$	6.2	11.6	13.3
	$K\beta_2$	12656.38(73)	17012.08(62)	
	$K\beta_2$	12655.11(33)	17015.30(49)	

observed FWHM is 1.63 eV, and, when this value is corrected for the instrumental function in this x-ray spectrometer [28], it becomes 1.58 eV. In Fig. 10, the spin doublet in Ca $K\beta_{1,3}$ spectra is about 0.7 eV from the logarithmic function. From Figs. 7 and 8, the corrected FWHMs of $K\beta_1$ and $K\beta_3$ diagram lines are about 0.8 and 0.7 eV, respectively. Assuming that the $K\beta_1$ and the $K\beta_3$ lines are separated by only 0.7 eV, the combined width becomes 1.5 eV, which matches the observed value. Therefore, the linear functions obtained in Figs. 7 and 8 are considered to be reliable.

In Table VI our experimental and theoretical results concerning $K\alpha_{1,2}$, $K\beta_{1,3}$, and $K\beta_2$ transition energies for Se, Y, and Zr have been compared with the results of other authors. Our theoretical predictions presented here have been determined in the framework of the MCDF method [52] and averaging over all the individual transitions within a given line. In what concerns the accuracy of our MCDF predictions, we estimate that the precision for the calculated values for the positions of the $K\alpha_1$, $K\alpha_2$, $K\beta_1$, $K\beta_3$, and $K\beta_2$ x-ray diagram lines is on the order of 0.2–0.5 eV [52]. This accuracy confirms the very good agreement between our theoretical and our experimental results. The photon energies of $K\alpha_{1,2}$ and $K\beta_{1,3}$ emission lines in the present paper are consistent with those of Bearden [29] and Deslattes *et al.* [51] and the energy value of our theoretical Y $K\beta_2$ spectral line, although consistent with our experimental value, disagrees with values of those authors [51].

The simulated shapes of the $K\beta$ lines of Se, Y, and Zr are presented in Fig. 3 and as can be seen, the overall agreement with the experimental data is very good for Se with a slight overestimation of the energy of the $[1s3d]$ satellite of around 4 eV. However, the calculated shake probabilities seem to agree very well for Se. For Zr, the intensity ratio of the multiplet agrees very well with the experimental data, but the calculated $[1s3d]$ shake probability is probably overestimated, leading to a shoulder on the high-energy side of the $K\beta_1$ peak,

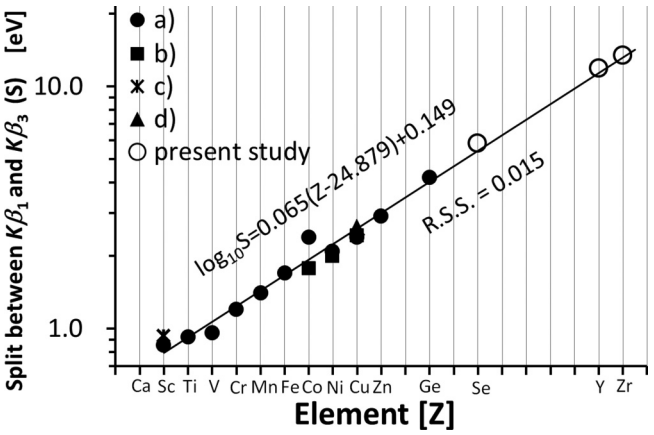

FIG. 10. The spin doublet energies of $K\beta_1$ and $K\beta_3$ lines for elements Se, Y, and Zr. The least-squares fitting was executed using both data in the present paper and Ito *et al.* [27]. (a) Ito *et al.* [27]. (b) Hölzer *et al.* [6]. (c) Anagnostopolos *et al.* [18]. (d) Pham *et al.* [26]. The value of the logarithmic function is well consistent with that in Ito *et al.* [27].

not visible in the measured spectrum. Furthermore, such as in Se, the satellite centroid is shifted towards the high-energy side of the x-ray diagram line. Still, the overall agreement of the line shape is very good. Regarding Y, the agreement is not as good as for Se and Zr as the $K\beta_3/K\beta_1$ ratio is around 10% lower than the experimental one, and for the shake structure, we find a similar behavior as in the Zr spectra with a consistent shake probability and a slight shift of the $[1s3d]$ satellite peak toward the high-energy side.

V. SUMMARY AND CONCLUSIONS

Se, Y, and Zr $K\alpha_{1,2}$ and $K\beta_{1,3}$ spectra were measured using a high-resolution two-crystal x-ray spectrometer. The values of the energies, FWHM, and ratio are compared with the literature and will contribute to future theoretical research in this field. The correction values for the FWHM of $K\alpha_1$ and $K\alpha_2$ agree well with the recommended full width at half maximum values of Campbell and Papp [46].

The values of the spin doublet in the $K\beta_{1,3}$ of Se, Y, and Zr are found to agree with the extrapolation of what has been reported by Ito *et al.* [27]. This is very important for the evaluation of the spin doublet observed by the x-ray spectrometer.

In what concerns the asymmetric index in the elements under study in this paper, the contribution of the $[1s3d]$ shake process is observed only for Se. However, on Y and Zr, the effect of the $[KN]$ and $[KO]$ shake processes increases, whereas the effect of $[KM]$ decreases. Therefore, it is difficult to confirm the existence of asymmetry.

The computed spectra in this paper required a huge computational effort due to the very large number of radiative and radiationless transitions. This high number of transitions is needed to calculate all of the parameters for a simulation of the multiplet line shapes in an *ab initio* way. The simulated spectra are in good agreement with the high-resolution experimental spectra from the double-crystal spectrometer although, for Y, the simulated line shape of the $K\beta_{1,3}$ multiplet presents a discrepancy on the intensity ratio of around 10%. From the theoretical results, we see that the $[1s3p]$ satellite lines might also contribute to the peak asymmetry of these elements, calling for more research on the simulation of other transition metals with Z higher than 40.

ACKNOWLEDGMENTS

This research was supported, in part, by Fundação para a Ciência e Tecnologia (Portugal) under Research Center Grants No. UID/FIS/04559/2020 (LIBPhys) and No. UID/MULTI/04046/2020 (BioISI), and by the Project No. PTDC/FIS-AQM/31969/201, "Ultra-high-accuracy x-ray spectroscopy of transition-metal oxides and rare earths." Laboratoire Kastler Brossel (LKB) is a Unité Mixte de Recherche de Sorbonne University-UPMC, de ENS-PSL Research University, du Collège de France et du CNRS No. 8552'. P.I. is a member of the Allianz Program of the Helmholtz Association, contract No. EMMI HA-216 "Extremes of Density and Temperature: Cosmic Matter in the Laboratory." P.I. acknowledges financing by the Programme Hubert Curien PESSOA 38028UD and Program No. PAUILF 2017-C08. This work was also supported by the National Science Centre (Poland) under Grant No. 2017/25/B/ST2/00901.

[1] J. Finster, G. Leonhardt, and A. Meisel, J. de Phys. Colloq. **32**, C4-218 (1971).
[2] B. Ekstig, E. Kallne, E. Noreland, and R. Manne, J. de Phys. Colloq. **32**, C4-214 (1971).
[3] M. Pessa, E.-K. Kortela, A. Suikkanen, and E. Suoninen, Phys. Rev. A **8**, 48 (1973).
[4] M. Deutsch, G. Hölzer, J. Härtwig, J. Wolf, M. Fritsch, and E. Forster, Phys. Rev. A **51**, 283 (1995).
[5] M. Deutsch, O. Gang, G. Hölzer, J. Härtwig, J. Wolf, M. Fritsch, and E. Forster, Phys. Rev. A **52**, 3661 (1995).
[6] G. Hölzer, M. Fritsch, M. Deutsch, J. Härtwig, and E. Forster, Phys. Rev. A **56**, 4554 (1997).
[7] M. J. Druyvesteyn, Z. Phys. **43**, 707 (1927).
[8] D. Doniach and M. Sunjic, J. Phys. C **3**, 285 (1970).
[9] K. Tsutsumi, J. Phys. Soc. Jpn. **14**, 1696 (1959).
[10] A. Meisel and W. Nefedov, Ann. Phys. (Leipzig) **464**, 48 (1961).
[11] A. Meisel and W. Nefedov, Ann. Phys. (Leipzig) **464**, 53 (1961).
[12] W. I. Nefedov, Bull. Acad. Sci. USSR, Phys. Ser. **28**, 724 (1964).
[13] K. Tsutsumi and H. Nakamori, in *X-ray Spectra and Electronic Structure of Matter*, edited by A. Faessler and G. Wiech (Fotodruck Frank OHG, Munchen, 1973).
[14] S. I. Salem, G. M. Hochney, and P. L. Lee, Phys. Rev. A **13**, 330 (1976).
[15] K. Tsutsumi, Y. Iwasaki, O. Aita, K. Ichikawa, and T. Watanabe, J. Phys. Soc. Jpn. **47**, 1920 (1979).

[16] K. S. Srivastava, R. L. Srivastava, O. K. Harsh, and V. Kumar, Phys. Rev. B **19**, 4336 (1979).
[17] K. S. Srivastava, S. Singh, A. K. Srivastava, R. S. Nayal, A. Chaubey, and P. Gupta, Phys. Rev. A **25**, 2838 (1982).
[18] D. F. Anagnostopoulos, R. Sharon, D. Gotta, and M. Deutsch, Phys. Rev. A **60**, 2018 (1999).
[19] C. T. Chantler, M. N. Kinnane, C.-H. Su, and J. A. Kimpton, Phys. Rev. A **73**, 012508 (2006).
[20] Y. Ito, T. Tochio, H. Ohashi, M. Yamashita, S. Fukushima, M. Polasik, K. Słabkowska, Ł. Syrocki, E. Szymańska, J. Rzadkiewicz, P. Indelicato, J. P. Marques, M. C. Martins, J. P. Santos, and F. Parente, Phys. Rev. A **94**, 042506 (2016).
[21] T. Ishizuka, T. Tochio, A. M. Vlaicu, D. Osawa, Y. Ito, T. Mukoyama, S. Hayakawa, Y. Gohshi, and T. Shoji, Adv. X-Ray Chem. Anal., Jpn. **30**, 21 (1998).
[22] W. C. Sauder, J. R. Huddle, J. D. Wilson, and R. E. Lavilla, Phys. Lett. A **63**, 313 (1977).
[23] R. D. Deslattes, R. E. LaVilla, and A. Henins, Nucl. Instrum. Methods, Phys. Res. **152**, 179 (1978).
[24] R. E. LaVilla, Phys. Rev. A **19**, 717 (1979).
[25] J. Bremer and H. Sorum, Phys. Lett. A **75**, 47 (1979).
[26] T. L. Pham, T. V. Nguyen, J. A. Lowe, I. P. Grant, and C. T. Chantler, J. Phys. B: At., Mol. Opt. Phys. **49**, 035601 (2016).
[27] Y. Ito, T. Tochio, M. Yamashita, S. Fukushima, A. M. Vlaicu, Ł. Syrocki, K. Słabkowska, E. Węder, M. Polasik, K. Sawicka, P. Indelicato, J. P. Marques, J. M. Sampaio, M. Guerra, J. P. Santos, and F. Parente, Phys. Rev. A **97**, 052505 (2018).
[28] T. Tochio, Y. Ito, and K. Omote, Phys. Rev. A **65**, 042502 (2002).
[29] J. A. Bearden, Rev. Mod. Phys. **39**, 78 (1967).
[30] M. H. Mendenhall, A. Henins, L. T. Hudson, C. I. Szabo, D. Windover, and J. P. Cline, J. Phys. B: At., Mol. Opt. Phys. **50**, 115004 (2017).
[31] J. Machado, C. I. Szabo, J. P. Santos, P. Amaro, M. Guerra, A. Gumberidze, G. Bian, J. M. Isac, and P. Indelicato, Phys. Rev. A **97**, 032517 (2018).
[32] J. Machado, G. Bian, N. Paul, M. Trassinelli, P. Amaro, M. Guerra, C. I. Szabo, A. Gumberidze, J. M. Isac, J. P. Santos, J. P. Desclaux, and P. Indelicato, Phys. Rev. A **101**, 062505 (2020).
[33] J. Machado, G. Bian, N. Paul, M. Trassinelli, P. Amaro, M. Guerra, C. I. Szabo, A. Gumberidze, J. M. Isac, J. P. Santos, J. P. Desclaux, and P. Indelicato, J. Phys. B: At., Mol. Opt. Phys. **52**, 215004 (2019).
[34] J. P. Desclaux, Comput. Phys. Commun. **9**, 31 (1975).
[35] P. Indelicato and J. P. Desclaux, Phys. Rev. A **42**, 5139 (1990).
[36] P. J. Mohr, G. Plunien, and G. Soff, Phys. Rep. **293**, 227 (1998).
[37] P. O. Löwdin, Phys. Rev. **97**, 1474 (1955).
[38] W. R. Johnson, *Atomic Structure Theory* (Springer-Verlag, Berlin/Heidelberg, 2007).
[39] E. J. McGuire, in *Atomic Inner-Shell Processes*, edited by B. Crasemann (Academic, New York/London, 1975), pp. 293–330.
[40] F. Bloch, Phys. Rev. **48**, 187 (1935).
[41] V. F. Demekhin and V. P. Sachenko, in *Röntgenspektren und Chemische Bindung*, 58 (VEB Repprocolor, Leipzig, 1966).
[42] T. Åberg, Phys. Lett. A **26**, 515 (1968).
[43] T. A. Carlson and C. W. Nestor, Phys. Rev. A **8**, 2887 (1973).
[44] L. G. Parratt, Phys. Rev. **50**, 1 (1936).
[45] Y. Gohshi, H. Kamada, K. Kohra, T. Utaka, and T. Arai, Appl. Spectrosc. **36**, 171 (1982)
[46] J. L. Campbell and T. Papp, At. Data Nucl. Data Tables **77**, 1 (2001).
[47] M. O. Krause and J. H. Oliver, J. Phys. Chem. Ref. Data **8**, 329 (1979).
[48] Y. Ito, T. Tochio, S. Fukushima, A. Taborda, J. M. Sampaio, J. P. Marques, F. Parente, P. Indelicato, and J. P. Santos, J. Quant. Spectrosc. Radiat. **151**, 295 (2015).
[49] A. Shigemi, T. Tochio, T. Ishizuka, N. Shigeoka, K. Ito, A. M. Vlaicu, Y. Ito, T. Mukoyama, and Y. Gohshi, X-Ray Spectrom. **28**, 478 (1999).
[50] Y. Ménesguen, M.-C. Lépy, Y. Ito, M. Yamashita, S. Fukushima, M. Polasik, K. Słabkowska, Ł. Syrocki, E. Węder, P. Indelicato, J. P. Marques, J. M. Sampaio, M. Guerra, F. Parente, and J. P. Santos, J. Quant. Spectros. Radiat. **236**, 106585 (2019).
[51] R. D. Deslattes, Ernest G. Kessler, Jr., P. Indelicato, L. de Billy, E. Lindroth, and J. Anton, Rev. Mod. Phys. **75**, 35 (2003).
[52] M. Polasik, Phys. Rev. A **39**, 616 (1989); **39**, 5092 (1989); **40**, 4361 (1989); **41**, 3689 (1990); **52**, 227 (1995); **58**, 1840 (1998).